Journal of Energy Challenges and Mechanics
http://www.nscj.co.uk/JECM/
ISSN 2056-9386
Volume 1 (2014) issue 2, article 1

Evolution of stress–strain state in structured rock specimens under loading until failure

结构化岩石样品加载失效前的应力—应变状态演变

V. N. Oparin, O. M. Usol'tseva, V. N. Semenov, and P. A. Tsoi

N.A. Chinakal Institute of Mining, Siberian Branch, Russian Academy of Sciences, Krasnyi pr. 54, Novosibirsk, 630091 Russia

usoltseva57@mail.ru

Accepted for publication on 22th July 2014

Abstract - **The comprehensive experimental studies into the change in the stress–strain state of rock specimens subjected to uniaxial loading until failure using automated digital speckle photography analysis shows that when stress reaches 50% of the limit strength of the specimens, low-frequency micro-deformation processes begin in the specimens under slow (quasi-static) stiff loading. The amplitude of the deformation-wave processes depends on the level of the pre-set macro-loading. Wave packets are plotted for averaged microstrains obtained in sandstone and marble specimens under uniaxial compression.**

In the elements of the scanned specimen surface in the region with the incipient crack, the microstrain rate amplitudes are a few times higher than in the undamaged surface region of the same specimen.

Keywords – **Rock mass, Hierarchical block structure, Laboratory experiment, Speckle photography method, Microstrains, Deformation-wave processes.**

I. INTRODUCTION

At the current stage, nonlinear geomechanics researchers place great emphasis on quantitative description of hierarchy of blocks in structure of rock masses [1]. This is important for delineation of clusters of structural blocks in the areas of nucleation of disastrous events and characterization of kinematics and dynamics of elastic energy accumulation and relaxation in such zones [2, 3].

Discovery of pendulum waves [4–6] transferred by structural blocks of different hierarchical levels in high-stress rock masses inspired a new theoretical research trend called geomechanical thermodynamics [7]. This research trend is directly associated with interpretation of transformation mechanism of potential (elastic) energy at nucleation sites of disastrous events (earthquakes, rockbursts, coal and gas outbursts) into kinetic energy of their fractals in clusters [1]. Based on that, it becomes possible to obtain an energy estimate of threshold values of deformation in check areas of rock masses or engineer constructions, when the threshold elevation will end up with destruction events in the high stress concentration zones in rocks.

The aim of this study was to analyze distribution and development of stress–stress state in structured rock specimens subject to uniaxial loading to failure. Specific attention was paid to possible oscillating motion of structural elements of the rock specimens under constraints (pre-set stresses at the boundaries of the specimens) and the kinetic energy fractals [8].

II. EXPERIMENTAL PROCEDURE AND MEASUREMENT EQUIPMENT

The experimental research used Instron-8802 servohydraulic testing machine for loading at the pre-set force and displacement and for the continuous recording of the load and the mobile grip displacement. Microstrains were recorded using automated digital speckle photography analyzer ALMEC-tv. The task is to interpret optical images of surface microrelief of a loaded specimen. The specimen surface is placed in the coherent radiation beam to obtain a speckle-picture. The speckles are "tight" to the corresponding points of the surface and reposition together with these points when the specimen is deformed. The displacements are recorded by frame-to-frame photography. All the parameters were recorded in real time, at frequency of 27 frames per second and spatial resolution not less than 1 μm. The processing output is the coordinates and displacements of the specimen surface points and timing, which allows calculating strain tensor components [3].

The uniaxial stiff compression used prismatic specimens of sandstone, marble and sylvinite, at the mobile grip displacement rate of 0.02–0.2 mm/min. Figure 1 illustrates testing of a marble specimen subjected to compression along long axis x at the grip displacement rate of 0.2 mm/min. the experiment lasted for 70 s. Ultimate strength of the specimen was 50.1 MPa, ultimate strain along x, measured by the machine cross beam unit displacement, was 0.059. Figure 2 shows the curves of the specimen stress and macrostrain and the specimen stress and time.

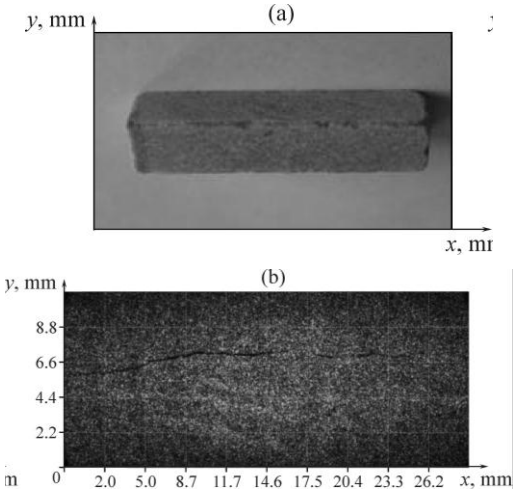

Fig. 1. (a) Marble specimen 47×11×10 mm and (b) its speckle-photography after fracture.

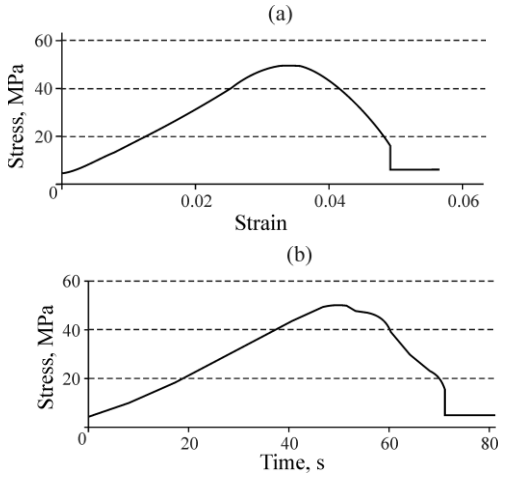

Fig. 2. (a) The curve of stresses and strain in the marble specimen in the direction of x and (b) the stress and time curve.

Concurrently with recording of microstrains on the specimen surface, measurement of vectors of microdisplacements at the surface points was carried out using ALMEC-tv. Having processed the results, we obtained a square grid of the surface displacements for the subsequent plotting of the strain tensor components.

III. Experimental Data Analysis

The experimental data analysis showed nonuniformity of plastic strain, starting from the onset of the rock specimen compression. In spite of the compression being uniaxial, at the constant rate of displacement of grips, the spatial–time field of the microstrains contain both shortening and elongation areas as seen in the scans of the specimen surface.

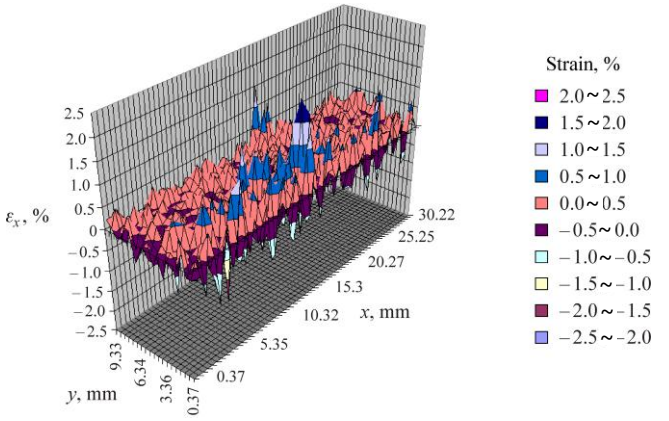

Fig. 3. Microstrains ε_x of the specimen surface at the moment of 30 s in the stress–time curve in Fig. 2.

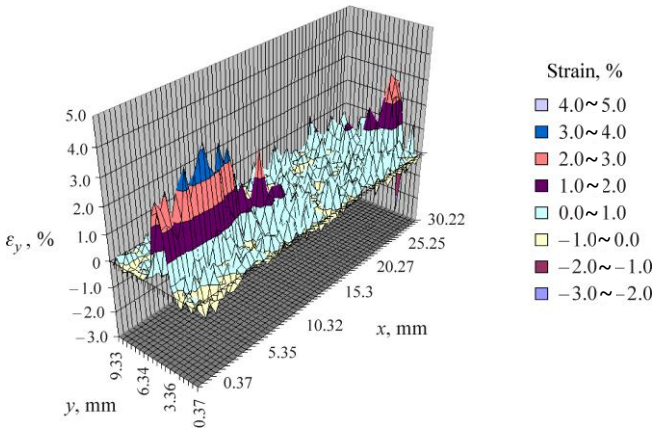

Fig. 4. Microstrains ε_y of the specimen surface at the moment of 30 s in the stress–time curve in Fig. 2.

Figure 3 and 4 show 3D diagrams, where the axes x and y are the specimen surface coordinates longitudinally and crosswise, and the z axis shows the microstrains at the fit point of the scanned surface. Figures 3 and 4 not only display the sign-alternating behavior of internal microstrain of the tested rock specimens but possible causes of the deformation, largely different from that is expected in the frames of the continuum mechanics. It is seen that apparent periods of oscillating strains fit with mineralogical and structural heterogeneities of the specimens (from fractions to a few millimeters in size). The level of the recorded strain (absolute values) is comparable with the geomechanical invariant $\mu_\Delta(\delta)$ [9]:

$$\mu_\Delta(\delta) = \frac{\delta_i}{\Delta_i} = \theta \cdot 10^{-2}\,,\ \theta \in \frac{1}{2}\sim 2\,,\ \forall i \qquad (1)$$

where δ_i—average width of joints of the structural rock-mass blocks with diameters Δ_i (i—hierarchy level).

IV. Stadiality of Micro- and Macro-Deformation of Rock Specimens under Uniaxial Loading until Failure and Low-Frequency Deformation-Wave Processes

"Stadiality" of deformation is a conventional notion, considering patterns of the rock mass stress and strain curves (e.g., Fig. 2). "Stages" are as a rule marked by "breakpoints" or noticeable change of the slope of the $\sigma - \varepsilon$ curve branches. Is it possible to find the other, objective methods to distinguish between deformation stages, for instance, with the help of dynamic–kinematic characteristics of local deformation-wave processes?

To answer the question above, we covered the load-exposed surface with a cross-hatch of rectangles (see Fig. 5) and calculated average microstrains for them in the directions of *x* and *y* (lengthwise and crosswise the specimen, respectively). Dimensions of the rectangles were chosen so that displacements at each point and averaged displacements differed not more than by 20–25%.

Figure 6 shows a fragment of variation in the averaged micros-strain. The time dependence of the longitudinal microstrain included compression and tension–compression. In Fig. 6, microstrains fluctuate around zero. It is seen that when macro-loading of the specimen reaches 25–30% of the uniaxial compression strength, inside the specimen a complex microdeformation-wave process begins.

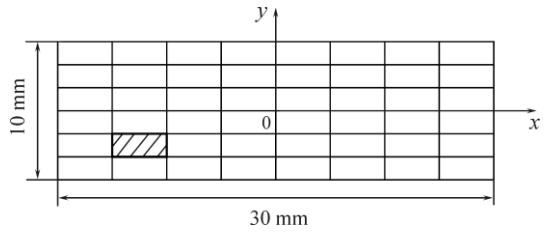

Fig. 5. Cross-hatch layout of the load-exposed surface of the test specimen: surface element (fragment) 3.5×1 mm is hatched.

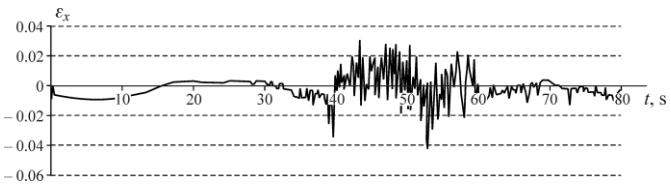

Fig. 6. Averaged microstrain ε_x of the surface element in longitudinal direction x.

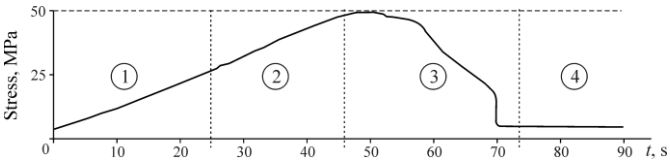

Fig. 7. "Stadiality" (stages 1–4) of the stress and loading time curve.

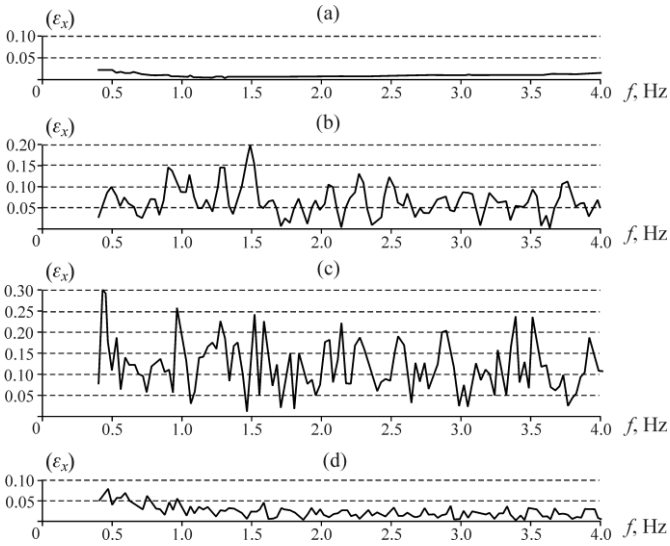

Fig. 8. Amplitude–frequency characteristic for the longitudinal microstrain ε_x by deformation stages: (a) stage 1; (b) stage 2; (c) stage 3; (d) stage 4.

The process of loading is conditionally split into four stages (Fig. 7): stage 1 and stage 2 are the load increase branch (stage 1 duration is to 0.5 of the peak load, stage 2 last up to the peak load); stage 3 is the post-peak branch; stage 4 is the residual strength branch. For each stage and for each surface element, we obtained deformation-wave packets by the averaged microstrains ε_x and ε_y and plotted the related amplitude–frequency characteristics from the Fourier transforms.

Figure 8 shows the amplitude–frequency characteristics for ε_x:

- at elastic deformation stage 1, under load under $0.5\sigma^v$ (σ^v—peak load), microstrain does not fluctuate;
- at stage 2, under the load increase from $0.5\sigma^v$ to the uniaxial compression strength of the specimen, microstrain oscillation starts, amplitudes of the oscillations grow and reach maximum values at post-peak loading stage 3;
- at residual strength stage 4, microstrain oscillation amplitudes decrease sharply (3–5 times) as against the previous two stages of deformation.

We performed checking calculation of frequencies based on the maximum values of deformation-wave amplitudes at the pre-failure and post-peak loading stages. Figure 9 shows the amplitude–frequency characteristics for the microstrain ε_x at deformation stage 2 for two different surface elements of a marble specimen. At the pre-failure stage, these frequencies

have values 0.9–1.1, 1.5, 2.3, 2.85, 3.75 Hz. The amplitude–frequency characteristics of ε_x at stage 3 are shown in Fig. 10; the frequencies to correspond to the maximum amplitudes are 0.45; 1; 1.6–1.7; 2.5–2.6; 2.9; 3.2; 3.5 Hz. Comparing the frequency ranges for stage 2 (0.9–3.75 Hz) and stage 3 (0.48–3.5 Hz), it is seen that the amplitude–frequency characteristics of the deformation-wave packets displace toward the lower-frequency range at stage 3. This complies with structure of wave packets of the EME recorded at the stage of rock failure [8].

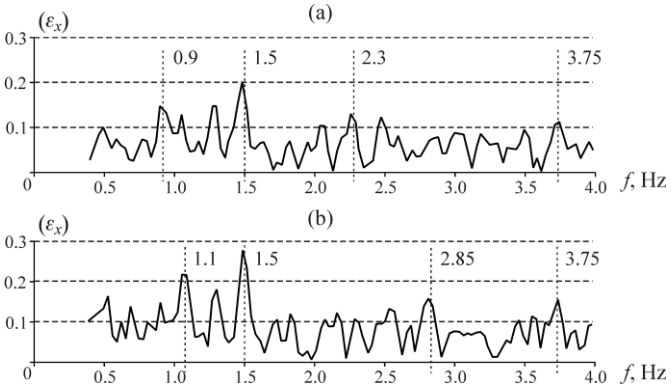

Fig. 9. Amplitude–frequency characteristics of the microstrain ε_x at deformation stage 2 for different surface elements (a) and (b) of marble specimen.

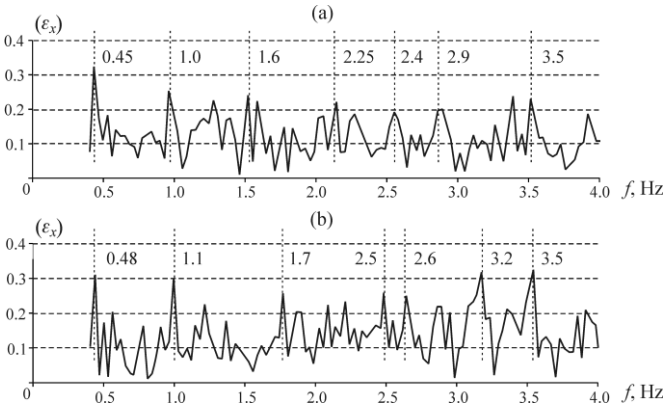

Fig. 10. Amplitude–frequency characteristics of the microstrain ε_x at deformation stage 3 for different surface elements (a) and (b) of marble specimen.

V. MICROSTRAIN RATE AT THE PRE-PEAK LOADING STAGE

We performed comparative calculations for two different regions on the scanned surface of the test specimen: region 1 is the region where crack originated and region 2 is the undamaged material (refer to Fig. 11). Each of regions 1 and 2 was divided into 120 elements 0.5×0.5 mm in dimension. For the elements, time dependences of the transverse strain ε_y were plotted. The microstrain rate estimation used approximation and smoothing of the experimental dependences $\varepsilon_y(t)$ for the mentioned elements within time interval 0 to 40 s. The trends of the $\varepsilon_y - t$ curves were calculated as the 6th order polynomials at the approximation accuracy 0.86–0.97. The functions of microstrain rates and time, $\varepsilon_y'(t)$, were calculated as the derivatives of the $\varepsilon_y - t$ trends.

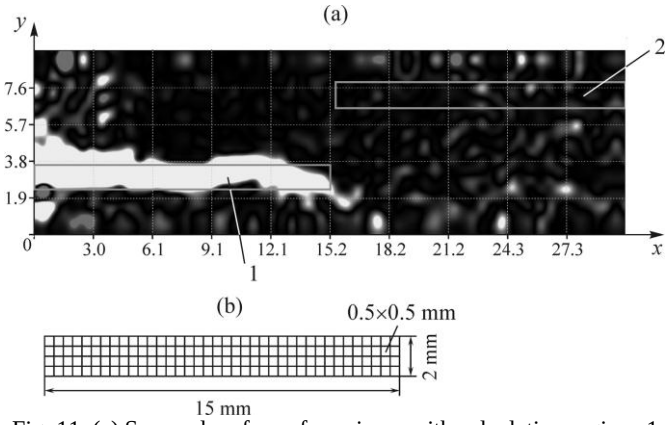

Fig. 11. (a) Scanned surface of specimen with calculation regions 1 and 2 and (b) parameters of the calculation regions.

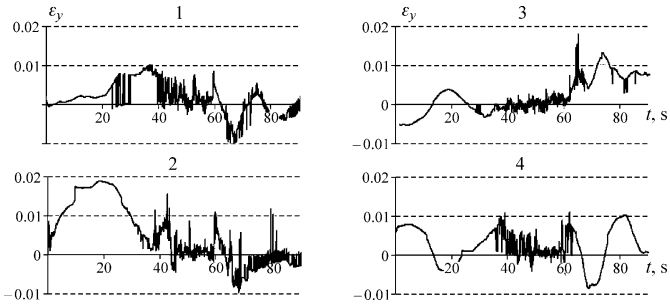

Fig. 12. Curves of the transverse microstrain ε_y and time for the elements 0.5× 0.5 mm in size in region 1 (where crack will originate later): 1, 2, 3, 4—arbitrary elements in the region.

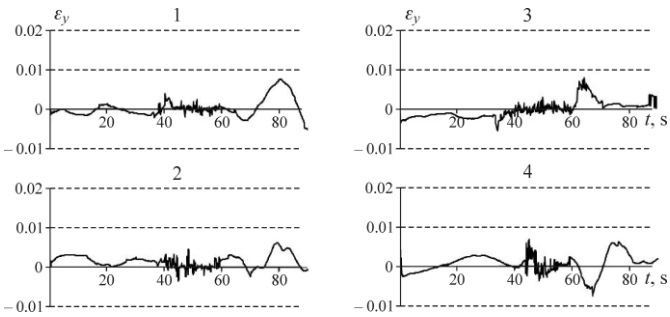

Fig. 13. Curves of the transverse microstrain ε_y and time for the elements 0.5× 0.5 mm in size in region 2 (undamaged).

Figures 12 and 13 show the representative curves of the transverse strains ε_y and time for arbitrary elements 0.5×0.5 mm in regions 1 and 2, respectively. In Fig. 12, 13 in the interval 0–40 s (which corresponds to the load ~42 MPa or 0.83 of the peak load), there are no high-frequency oscillations of the microstrains.

Figures 14 shows the curves of the transverse microstrain rate and time for elements 1, 2, 3, 4, 0.5× 0.5 mm in size in region 1, where crack originated and region 2 is the undamaged material. As follows from Fig. 14, the amplitudes of the microstrain rates are a few times higher in the elements of the region with incipient crack than in the undamaged region (regions 1 and 2, respectively). Sometimes, the rate grows under the higher loading.

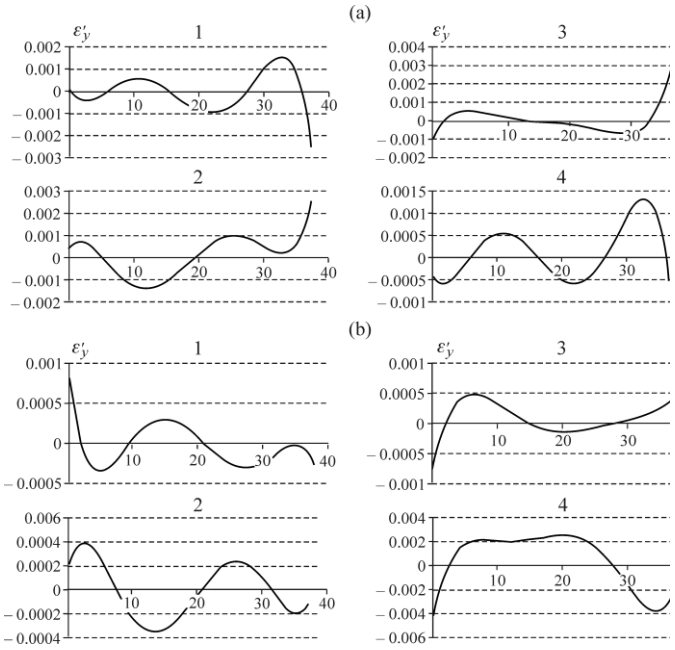

Fig. 14. The curves of the transverse microstrain rate and time for elements 1, 2, 3, 4 0.5×0.5 mm in size in (a) region 1 and (b) region 2.

VI. Conclusion

The detailed studies into the micro-level stress–strain state distribution and propagation over acting faces of rock specimens subject to uniaxial loading until failure, using automated digital speckle photography analyzer ALMEC-tv, have shown that:

- under uniaxial stiff loading of prismatic sandstone, marble and sylvinite specimens on the Instron-8802 servohydraulic testing machine at the mobile grip displacement rate 0.02–0.2 mm/min, at a certain level of stressing, low-frequency micro-deformation processes originate in the specimens due to slow (quasi-static) force;

- the amplitude of that deformation-wave processes greatly depends on the micro-loading stage:

—at the elastic deformation stage, under the specimen stress lower than half ultimate strength of the specimen, there are no oscillations of microstrains;

—at the nonlinearly elastic deformation stage, under stress varied from 0.5 to 1 ultimate strength of the specimens, the amplitudes of microstrains grow, including the descending stage 3; the oscillation frequency $f = 0.5 - 4$ Hz;

—at the residual strength stage, the amplitudes of the microstrains drop abruptly (3–5 times) as against stages 2 and 3;

- in the elements of the scanned specimen surface in the region with the incipient crack, the microstrain rate amplitudes ε'_y are a few times higher than in the undamged surface region of the same specimen. Sometimes, deformation rate greatly grows with increase in the load.

In conclusion, it has been experimentally proved that under certain loading of rock specimens, the oscillations of fractals or other structural inhomogeneities begin much earlier than the ultimate unaixail compression strength is reached. The authors think, the deformation-wave processes inside rocks and rock masses are tightly connected with the seismic and electromagnetic emissions, that are associated as well. Rock masses may be where displacement of fracture edges is "electromagnetically" connected with the pendulum deformation-wave processes [1, 8]. assessed as "capacitors" with intrinsic structural hierarchy, where displacement of fracture edges is "electromagnetically" connected with the pendulum deformation-wave processes [1, 8].

VII. Acknowledgments

The work was supported by partly the Russian Academy of Sciences, project ONZ-RAN 3.1, grant no. 12-05-01057. The equipment is kindly provided by the Shared Geomechanical, Geophysical and Geodynamic Measurement Center of the Siberian Branch of the Russian Academy of Sciences.

References

[1] V.N. Oparin and A.S. Tanaino. Canonical Scale of Hierarchy Presentation in Science on Rocks (Kanonicheskaya shkala ierarkhicheskikh predstavlenii v gornom porodovedenii), Novosibirsk: Nauka, 2011.

[2] V.N. Oparin, A.D. Sashurin, A.V. Leont'ev. Modern Geodynamics of the Outer Crust of EarthL Sources, Parameters, Impact (Sovremennaya geodinamika massiva gornykh porod verkhnei chasti litosphery: istoki, parametry, vozdeistvie na ob'ekty nedropol'zovaniya), Novosibirsk: SO RAN, 2008.

[3] O.M. Usoltseva, L.A. Nazarova, P.A. Tsoi, L.A. Nazarov, and V.N. Semenov. "Genesis and Evolution of Discontinuities in Geomaterials: Theory and a Laboratory Experiment", *Journal of Mining Science*, vol. 49, no. 1, pp. 1–7, 2013.

[4] V.N. Oparin. "Scientific Discoveries in Geomechanics at the Turn of a Century and Their Application Outlook", *Proc. Int. Conf. Geodynamics and Stress State of the Earth's Interior*, Novosibirsk: IGD SO RAN, 2008.

[5] V.V. Adushkin and V.N. Oparin. "From the Alternating-Sign Explosion Response of Rocks to the Pendulum Waves in Stressed Geomedia. Part I", *Journal of Mining Science*, vol. 48, no. 2, pp. 203–222, 2012.

[6] V.V. Adushkin and V.N. Oparin. "From the Alternating-Sign Explosion Response of Rocks to the Pendulum Waves in Stressed Geomedia. Part II", *Journal of Mining Science*, vol. 49, no. 2, pp. 175–209, 2013.

[7] V.N. Oparin. "Pendulum Waves and "Geomechanical Temperature", *Proc. 2nd Russia–China Conf. Nonlinear Geomechanical–Geodynamic Processes in Deep Mining*, Novosibirsk: IGD SO RAN, 2012.

[8] V.N. Oparin, G.N. Yakovitskaya, A.G. Vostretsov, V.M. Seryakov, and A.V. Krivetsky. "Mechanical–Electromagnetic Transformations in Rocks on Failure", *Journal of Mining Science*, vol. 49, no. 3, pp. 343–356, 2013.

[9] M.V. Kurlenya, V.N. Oparin, and A.A. Eremenko. Relation of Linear Block Dimensions of Rock to Crack Opening in the Structural Hierarchy of Masses, *Journal of Mining Science*, vol. 29, no. 3, pp. 197–203, 1993.

[10] V.N. OparinA.P. , Tapsiev, V.I. Vostrikov al. "On Possible Causes of Increase in Seismic Activity of Mine Fields in the Oktyabrsky and Taimyrsky Mines of the Norilsk Deposit in 2003. Part I: Seismic Regime", *Journal of Mining Science*, vol. 40, no. 4, pp. 321–338, 2004.

[11] Oparin, V.N., Kozyrev, A.A., Sashurin, A.D., et al. Erath Crust Destruction and Self-Organization in the Areas Exposed to Heavy Impact of Mining (Destruktsiya zemnoi kory i protsessy samoorganizatsii v oblastyakh sil'nogo tekhnogennogo vozdeistviya), Novosibirsk: SO RAN, 2012.

[12] Kurlenya, M.V., Oparin, V.N., and Eremenko, A.A., "Mine Seismic Data Scanning Method", *Reports of Academy of Sciences*, Vol . 333, no. 6, pp. 784-787, 1993.